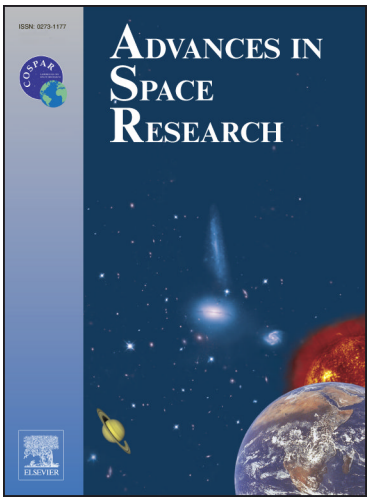

Altimetry-based sea level trends along the coasts of Western Africa

Florence Marti, Anny Cazenave, Florence Birol, Marcello Passaro, Fabien Léger, Fernando Niño, Rafael Almar, Jérôme Benveniste, Jean François Legeais

PII: S0273-1177(19)30360-6
DOI: https://doi.org/10.1016/j.asr.2019.05.033
Reference: JASR 14274

To appear in: *Advances in Space Research*

Received Date: 24 February 2019
Revised Date: 8 May 2019
Accepted Date: 20 May 2019

Please cite this article as: Marti, F., Cazenave, A., Birol, F., Passaro, M., Léger, F., Niño, F., Almar, R., Benveniste, J., François Legeais, J., Altimetry-based sea level trends along the coasts of Western Africa, *Advances in Space Research* (2019), doi: https://doi.org/10.1016/j.asr.2019.05.033

Altimetry-based sea level trends along the coasts of Western Africa

Florence Marti[1], Anny Cazenave[1], Florence Birol[1], Marcello Passaro[2], Fabien Léger[1], Fernando Niño[1], Rafael Almar[1], Jérôme Benveniste[3] and Jean François Legeais[4]

1. LEGOS, 18 avenue Edouard Belin, 31401 Toulouse Cedex 9, France
2. DGFI-TUM, Arcisstrasse 21, Munich, 80333, Germany
3. ESA-ESRIN, via Galileo Galilei, Frascati, I-00044, Italy,
4. CLS, 8-10 rue Hermes, 31520 Ramonville St Agne, France

Submitted to **Advances in Space Research**

Special Issue '25 years of satellite altimetry'

2nd Revision

7 May 2019

Abstract

We present results of contemporary coastal sea level changes along the coasts of western Africa, obtained from a dedicated reprocessing of satellite altimetry data done in the context of the ESA 'Climate Change Initiative' sea level project. High sampling rate (20 Hz) sea level data from the Jason-1 and Jason-2 missions over a 14-year-long time span (July 2002 to June 2016) are considered. The data were first retracked using the ALES adaptative leading edge subwaveform retracker. The X-TRACK processing system developed to optimize the completeness and accuracy of the corrected sea level time series in coastal ocean areas was then applied. From the 14-year long sea level time series finally obtained, we estimate sea level trends along the Jason-1 & 2 tracks covering the study region. We analyze regional variations in sea level trends, with a focus on the changes observed between the open ocean to the coastal zone. Compared to the conventional 1 Hz sea level products dedicated to open ocean applications, the retracked 20 Hz measurements used in this study allow us to retrieve valid sea level information much closer to the coast (less than 3-4 km to the coast, depending on the satellite track location). The main objective of this study is twofold: (1) provide sea level products in the coastal areas from reprocessed altimetry data and (2) check whether sea level changes at the coast differ from that reported in the open ocean with conventional altimetry products. In the selected region, results show that over the study period, sea level trends observed near the coast of western Africa are significantly different than offshore trends. In order to assess the robustness of the results, detailed analyses are performed at several locations to discriminate between possible drifts in the geophysical corrections and physical processes potentially able to explain the sea level changes observed close to the coast.

1. Introduction

Coastal zones are among the most populated regions of the world. Being located at the interface between land and sea, they are exposed to a variety of natural and man-made hazards, e.g., extreme weather such as damaging cyclones, storm surges and associated inundations, sea level change, extreme river discharge, destruction of ecosystems, water pollution, salt water intrusion into coastal aquifers, vertical land motions, etc. They are also impacted by direct human activities, such as increasing urbanization, coastal & river engineering, land use change, subsidence due to groundwater pumping in coastal megacities and oil extraction on shallow shelves. Many shorelines are currently eroding (25% of sandy beaches worldwide and 75% in northern Europe; Luijendijk et al., 2018). This raises the question of understanding the underlying causes. It is not yet fully clear whether reported broad-scale erosion is due to natural processes only, to direct human activities or to the combination of both. The contribution of present-day sea level rise to shoreline retreat has not yet been fully assessed, except at a few limited locations where detailed studies have been conducted (e.g., Le Cozannet et al., 2013). This mostly results from limited knowledge about coastal sea level changes. Indeed, there are reasons to believe that sea level changes at the coast significantly deviate from open ocean changes. A number of small-scale processes of oceanographic and hydrological origin, specific to coastal areas, may indeed modify the rate of sea level rise near the land: e.g., continental slope and shelf currents, changes in the wave characteristics, fresh water input from rivers in estuaries, etc. (Woodworth et al., 2019). Hence, sea level change at the coast may not just be an extrapolation of the regional sea level trends that are routinely provided by standard ocean altimetry products (see **Fig.1**, showing a global map of altimetry-based sea level trends over 2002-2016 -our study period-, based on the altimetry products from the Copernicus Climate Change Service).

Tide gauges are located at the coast, thus are in principle able to provide information on coastal sea level. However, while the mid latitude regions of the northern hemisphere are rather well covered, this is not the case for a numbered of world coastlines where tide gauges are either lacking or the data are not available. This is particularly true along the coasts of western Africa (see **Fig.2** showing the GLOSS tide gauge network; https://www.psmsl.org/products/gloss/status) where only Dakar (Senegal) displays a long sea level record.

Since the early 1990s, sea level changes are estimated at global and regional scales using high precision satellite altimetry (e.g., Escudier et al., 2018, Legeais et al., 2018, Cazenave et al., 2018). However, classical altimetry processing and products provide sea level data up to 10-15 km from the coast only (Cipollini et al., 2018, Benveniste et al., 2019). The main limitation comes from the land contamination within the footprint of the radar signal reflected from the Earth surface, leading to radar echoes (or waveforms) that are significantly different from those collected over pure ocean surfaces. Estimating the range (the distance between the satellite and the Earth surface) in such environments is thus complex (see an illustration in **Fig.3**). In addition, the geophysical corrections to be applied to the altimetry measurements (e.g., wet tropospheric correction, sea surface bias, ocean tides, etc.) are optimized for the open ocean and so far, may remain a source of significant errors in the coastal zones.

Nevertheless, it has been shown that it is possible to retrieve significantly more valid sea level data in the coastal zones by using adapted reprocessing of the altimetry-based measurements in order to extract a robust estimate of the 'range' from the radar echoes (a process called 'retracking'; Gommenginger el al., 2011; Passaro et al., 2015; Wang and Ichikawa, 2017; Xu et al., 2018). In parallel, the quality of geophysical corrections is also constantly improved (Cipollini et al., 2017; Fernandez and Lazaro, 2016) and solutions exist to reduce the associated remaining errors in the coastal domain (Birol et al., 2017).

In this paper, we have combined both approaches to process a dedicated new coastal sea level dataset and present sea level trend results along the coasts of western Africa using Jason-1 and Jason-2 altimetry over 2002-2016. The results presented here are an outcome of a project supported by the European Space Agency (ESA) in the context of the Climate Change Initiative (CCI) sea level project (http://www.esa-sealevel-cci.org/).

2. The ESA CCI Sea level project and its extension to coastal zones.

Earlier this decade, ESA implemented the Climate Change Initiative project (http://cci.esa.int/) dedicated to provide long, accurate time series of a set of Essential Climate Variables (ECVs) observable from space, as defined by the Global Climate Observing System (GCOS, 2011) to monitor and understand climate change. The first phase (2011-2017) of the CCI project allowed the processing of 13 ECVs, including sea level, using all available satellite data sets. Within the CCI sea level project (noted SL_cci), 9 different satellite altimetry missions were reprocessed, and new, optimized algorithms and geophysical

corrections were developed for the production of an accurate gridded sea level time series at monthly interval over 1992-2015. This product has been shown to be significantly improved and more suitable for climate studies, in comparison to previous altimetry-based sea level data sets, approaching the GCOS requirements in terms of accuracy and stability (Legeais et al., 2018). In particular, the uncertainty of the global mean sea level trend, now at the level of ~ 0.3 mm/yr, has been significantly reduced (Ablain et al., 2017). At regional scale, sea level trend errors have also been reduced by 1 to 2 mm/yr. The sea level ECV (at global and regional scales) is now operationally produced by the Copernicus Climate Change Service (C3S), adopting the altimetry standards developed in the SL_cci project.

In the context of additional activities of the CCI Sea Level project, it has been proposed to extend the processing efforts done during the SL_cci project to the coastal zones, and to develop new coastal sea level products for estimating rates of sea level change in selected regions. Such a new data set would help answering the following questions:

(1) Is sea level rising at the same rate at the coast as in the open ocean?

(2) Does the answer to question (1) depends on the region considered?

(3) How small-scale ocean dynamics impact sea level variations and trends at the coast?

(4) What is the influence on coastal sea level of fresh water input from rivers in estuaries?

(5) Is present-day shoreline erosion due to sea level rise or not?

The delivery of coastal sea level products, that include most recent algorithms developments, will allow better understanding of the role of climate-related sea level rise on present-day coastal changes and impacts.

In this study, we focus on the Western African region (indicated by the green square in Fig.1). Two main reasons justify this choice: (1) the Western African coastal region is highly populated and threatened by climate change and human-induced forcings, and (2) in situ tide gauge networks are very sparse (almost inexistent). The Western African coastal zone consists of a narrow, low-lying belt where a large percentage of the population lives in coastal megacities (e.g., Dakar, Conakry, Abidjan, Accra, Lagos, and Douala). In between these big cities, a large number of intermediate size cities have developed, e.g., in Senegal, Ivory coast, Togo, Benin, Nigeria and Cameroon. In Nigeria, about 20 million people live close to the coast. In Senegal, about 5 million people live in Dakar and 90% of industries are located within the Dakar coastal zone (Wong et al., 2014). In Ghana, Benin, Togo and Nigeria, most economic activities are also located in the coastal zone. Because these urban centres stand on low-lying sandy coasts, they are particularly vulnerable to marine hazards, including sea level rise (Brown., 2011, Neumann et al., 2015; Dada et al., 2019). The recently observed increase

in shoreline erosion has become a major issue (Ndour et al., 2018; Almar et al., 2015; Giardino et al., 2018; Anthony et al., 2019) but it remains unclear if this is due to sea level rise or human activities (e.g., sand extraction). Moreover, flooding events are becoming more frequent (Angnuureng et al., 2018; Almar et al., 2019). It is urgent to systematically monitor sea level at the coast to better understand its current behaviour and provide insight on future changes (Abessolo Ondoa et al., 2017; 2019). Unfortunately, the West African coastlines are almost devoid of tide gauges. The few existing records are very short and suffer from many data gaps, preventing from estimating decadal or longer-term sea level trends at the coast. A single long-term record is available at Dakar (Senegal), although it is affected by an important data gap in the middle of the altimetry period.

For all these reasons, estimating coastal sea level changes in this region with satellite altimetry is an important goal. It is the purpose of the present study.

3. Data and Method

3.1 Data

In this study, we considered along-track, high-resolution (i.e., at 20 Hz, corresponding to a resolution of ~350 m between consecutive measurements) sea surface height data from the Jason-1 and Jason-2 missions over the July 2002 to June 2016 time span (full 14-year long time span).

The sea level data are derived from range values retracked with the ALES adaptative leading edge sub-waveform system developed by Passaro et al. (2014) to improve the number and quality of coastal sea level estimates from altimetry, and provided by the Technical University of Munich (TUM). The ranges from ALES have been then processed by the X-TRACK software developed by the CTOH (Centre de Topographie de l'Océan et de l'Hydrosphère) at the LEGOS (Laboratoire d'Etudes en Géophysique et Océanographie Spatiales) laboratory, in order to obtain corrected sea level times series along a nominal ground-track (Birol et al., 2017). Initially, X-TRACK was designed to provide along-track sea surface height time series at 1-Hz for different conventional nadir altimetry missions (Topex/Poseidon, GFO, Envisat, Jason-1, Jason-2, Jason-3 and SARAL/AltiKa). For the purpose of the present study, it has been adapted to the processing of the 20-Hz ALES data (Birol et al., in preparation). Once the altimetry waveforms have been retracked with ALES, combining with the X-TRACK processing system ensures quality of the resulting coastal sea level time series. Briefly, the method adopted consists in analysing the behaviour of the different altimeter geophysical

corrections as a whole and then editing and recomputing the suspicious correction values in order to maximize the number of valid near-shore sea level data. This is particularly true for the wet tropospheric correction derived from the radiometer. The rapid and unrealistic variations observed near the coast in the original wet tropospheric correction are largely attenuated after this correction editing process (note that since GPS stations are almost inexistent along the coasts of Western Africa, there is no advantage of using here the GPD+ correction developed in the context of the CCI sea level project) .More details about X-TRACK are provided in Birol et al. (2017).

Table 1 summarizes the geophysical corrections applied to the 20 Hz Jason-1 and Jason-2 data. The sea state bias (SSB) correction is computed at 20 Hz during the ALES retracking process (Passaro et al., 2018). Other corrections are provided at 1 Hz and further interpolated at 20 Hz.

Corrections	**Jason-1**	**Jason-2**
Ionosphere	From dual-frequency altimeter range measurements	
Dry troposphere	From ECMWF model	
Wet troposphere	From radiometer	
Sea state bias (SSB)	ALES SSB (Passaro et al., 2018)	
Solid tides	From tidal potential model (Cartwright and Taylor, 1971)	
Pole tides	From Wahr (1985)	
Loading effect	From FES 1999 (Lefèvre et al., 2002)	
Dynamic Atmospheric Correction	TUGOm 2D global models for periods smaller than 20 days (Carrere and Lyard, 2003) + Inverted barometer for periods greater than 20 days, derived from ECMWF pressure fields.	
Ocean Tide	FES 2012 (Carrere et al., 2012)	

Table 1: List of corrections used in the computation of X-TRACK/ALES sea level data.

The sea level data, not exactly located at the same position from one cycle to the other, were then projected onto equally-spaced reference points along a ‘mean’ reference ground-track by the X-TRACK software (after the editing step). Time series of sea level anomalies –SLA- (with respect to the mean reference track) were then finally estimated (i.e., differences between individual cycle corrected sea level data projected on the corresponding nominal point of the reference track and the mean sea level value estimated at this nominal point).

Jason-1 and Jason-2 data were then merged to obtain a single SLA time series. To do this, a bias between both missions was estimated at regional scale. The procedure adopted consisted in:

(1) Calculation of the mean sea level over the region considered for both Jason-2 cycles 1 to 19 and Jason-1 cycles 240 to 258, excluding all data located at a distance < 50 km from land and altimetry points where less than 80% valid sea level data,

(2) Calculation of the difference between the resulting Jason-2 and Jason-1 mean sea levels. The Jason-1 SLAs were then extended by the Jason-2 time series, as of Jason-2 cycle 21, after subtracting the regional bias to Jason-2 SLAs.

In the following, all results presented are based on the resulting combined dataset, called X-TRACK/ALES SLA.

Apart from the product described above and developed for this project, we also considered the multi-mission gridded product provided by the Copernicus Climate Change Service (C3S) (https://climate.copernicus.eu/), in order to estimate the regional sea level trends for the period 2002-2016. The C3S product is a multi-mission, merged gridded product with a 1/4° spatial resolution. Thus, small scale coastal processes are not expected to be resolved with the same performance as with high resolution 20 Hz along-track measurements. However, the C3S product is helpful to show regional (open ocean) sea level trends in the study region. The corresponding trend map is shown in **Fig.4** over the western tropical Atlantic. The Jason tracks are superimposed.

Finally, to locate the western African coastline, we considered the GSHHS (Global Self-consistent, Hierarchical, High-resolution Shoreline Database) data base **(**Wessel and Smith, 1996; http://www.soest.hawaii.edu/wessel/gshhg/), providing geographical coordinates of the coastline. This data set is based on multiple sources. Its accuracy in the study region is not well known (W.H Smith and P. Wessel, personal communications) but a comparison with the coastline position from Google map images shows differences of less than 100 m in the study area.

3.2 Estimate of open ocean and coastal sea level trends along the Jason-1/2 tracks: Method

We computed sea level trends over the 14-year period considered in this study along all Jason tracks of the study region. For each track, sea level trends were computed over successive segments of varying lengths along different portions of the reference track from the open ocean to the coast. Constant length segments were considered along the tracks, starting from the closest 20 Hz point to the coast. The construction of the segments along each track is

illustrated in Fig.5. The computation of the distance of each 20 Hz point to coast used the GSHHS data base.

To spatially average the data over a given segment, a first method would be to sort all the 20 Hz points with respect to their distance to the nearest coast (defined by GSHHS), and gather them in bins of constant length (e.g. [0 – 2km], [2 – 4 km]...). In this case, one bin may include two measurement points located in the same distance range from the shore but with completely different latitudes (e.g. if a track passes nearby an island).

For this reason, we applied a second method, as illustrated in **Fig.5**: for each track, the altimetry point closest to the coastline (coastline position derived from the GSHHS data base), considered valid after the data editing process was used as starting point to build the segments backward along the track. Taking into account its own distance to the coast, we computed a second distance to coast data for all following 20 Hz points. Then, various 20 Hz points were gathered to form constant length segments along the track. The mean position of each along-track segment was defined by the location of the closest 20 Hz point to the middle of the segment.
We successively considered three spatial scales to estimate the along track evolution of the sea level trends:

a) **The entire track over the selected region**; Trends were then computed along 50 km-long successive segments by averaging all SLA data within the segment.
b) **The first 50 km from the coast**; Trends were computed along 2 km-long segments. As for the 50 km-long segments, all SLAs in the segment were averaged to compute the trend.

An additional case (c) was considered:

c) **The first 15 km from the coast**; Trends were computed at individual 20 Hz point location.

For each case (a), (b) or (c), all orbital cycles from July 2002 to June 2016 were considered and SLA data were averaged on a monthly basis. A mean SLA value was computed over the study period and removed from each individual SLA. For cases (a) and (b), the SLA data

were spatially averaged along the segment length for each orbital cycle. Removal of annual and semi-annual signals was performed, using a simple least-squares fit to sinusoidal functions, before computing trends. The trend computation was based on a simple linear regression fit.

4. Open ocean and coastal sea level trends along the Jason-1/2 tracks in the western African region

4.1 Results

Sea level trend were estimated for each of the 23 Jason-1/2 tracks covering the western African region. For each track, we computed sea level trends over the 14-year time span at each 20 Hz point for the closest track portion to the coast (a few km).

Fig. 6, 7 and 8 show computed along-track trends and associated uncertainties (+/- 1 standard error) at each valid 20 Hz point, for 3 ascending tracks (numbered 187, 237 and 33) selected as examples. The background maps show the geographical setting based on a 2018 version of Google Earth. Track 187 is an ascending satellite track crossing land just south of Freetown in Sierra Leone. Track 237 crosses land east of Abidjan in Ivory Coast, not far from the Ghana border and track 33 crosses land east of Port Harcourt in Nigeria. On each figure, colors correspond to trend/error values. When present, red & white triangles identify points with non-significant trend estimates (sea level time series at each 20 Hz point data too scattered or not enough numerous for a robust trend estimation; see below). Note that the color scales for sea level trends and trend errors are different.

To check the robustness of estimated trends, in particular the closest to the coast, we plotted the sea level time series over the study period for the first few points closest to the coast. These are shown for each track below the Google map plots in Fig.6-8. Red dots correspond to outliers identified by a simple 2-sigma statistical test. They were discarded for the trend computation. The solid line is the regression line computed over the 14-year time span (excluding the outliers). The corresponding trend value and associated error (defined as +/-1 standard deviation) are indicated in the legend of each figure. We note that the 20 Hz time series show good continuity and little scatter, providing confidence in the computed trends.

Fig. 9, 10 and 11 present another set of 3 examples along descending tracks numbered 174, 46 and 20. Track 174 crosses the land-sea interface south of Dakar (Senegal). Track 46 reaches the sea right east of Accra (Ghana). Track 20 is a short track crossing the land-sea

interface in Cameroon. In Fig.11, results are shown for the northern portion of track 20 (called 20N) crossing land northwest of Douala. As in Fig. 6-8, these figures show along-track trends and uncertainties at successive 20 Hz points superimposed on a Google map, as well as associated SLA time series of the first three valid points closest to the coast.

We also computed trends for each 20 Hz point located within 15 km from the coast. These are presented in **Fig. 12** as a function of distance to the coast (in Fig.12, 24 trend plots are shown corresponding to the 23 tracks, but with two portions for track 20: north and south, called 20N and 20S). Trend errors (+/- 1 sigma) are also indicated. First, we note good continuity of estimated trends from offshore to the coast. We also note quite different behaviors from one track to another when approaching the coast. In most instances, we observed a trend increase in the last few km towards the coast. Some tracks show slight trend decrease followed by a sharp increase when approaching the coast (e.g., tracks 9, 85, 161 and 237). Some others show continuous trend increase over the 15-km distance to coast (e.g., tracks 111, 187, 109, 185, 20N, 122, 46, 224, 72, 174). Others show either no trend increase (e.g., tracks 35, 33, 7 and 198) or trend decrease (e.g., track 135 and 211). The observed trend decrease along track 211 looks rather continuous within 5 km to the coast. This track crosses the coast very close to the Niger River estuary in Nigeria, hence the decrease in trend may reflect real coastal signal associated with the river impact on coastal waters (see discussion). In most cases, the trend values deviate significantly within 5 km to the coast compared to those computed farther to the coast.

From Fig. 6 to 12, we note that trend errors tend to increase when approaching the coast. To illustrate this more clearly, Fig.13 shows for two tracks chosen as examples (tracks 187 and 20N), trend errors computed at each 20 Hz point over the last 50 km to coast. Errors are on the order of 1 mm/yr in the open ocean, then increase over the last 10 km to coast. However, in terms of signal to noise ratio, very close to the coast computed trends remain significant, even if errors are larger.

4.2 Closest distances to coast and associated sea level trends

The results presented above show that depending on the Jason track, it is possible to estimate reliable sea level trends as close as 2-4 km to the coast. This is illustrated by **Fig. 14** showing the closest distance to the coast reached for the first valid point. From Fig.14, we note that

there is no systematic effect depending on the track direction (ascending and descending). From the 24 tracks covering the study region, 19 of them provide valid trends at distances less than 3 km to the coast. For 9 of them, the distance is even shorter (< 2 km), with as many ascending than descending tracks. For 3 tracks, the distance is ~1 km or less.

Associated trends are shown in Fig. 15a. Most of them are positive; 17 over 24 cases display trends > 5 mm/yr and for 3 of them trends are >10 mm/yr. Only 4 trends are negative. It is worth noting however that the study period is short (14 years) and by no means what is measured here, represents long-term climate-related sea level trends. Nevertheless, even if the computed trends result from decadal variability, they have large enough amplitude to locally impact the coastal zone on decadal time scale.

We also compared the trends derived from the high-resolution XTRACK/ALES data with trends computed with the C3S gridded products. For that purpose, we interpolated the C3S gridded data along each Jason track. **Fig.16** shows sea level trends averaged over 50 km-long segments along track 148 (chosen as an example), as a function of distance to the coast. The C3S trends interpolated along the track are superimposed. As expected, the latter are smoother but the same large-scale behaviors are seen in both data sets. Fig.16 also shows the same but for 2 km-long segments over the last 50 km to the coast. In that case, the C3S trends are constant, unlike the trends based on the new X-TRACK/ALES product, indicating that these new data indeed contain small-scale local variability information that the gridded data are unable to capture.

In Fig.15b, we plotted the distribution of trends at the shortest distance to coast based on the gridded C3S data interpolated along each track. In that case, the closest distance to coast is on the order of 25 km (the mesh size of the C3S grid). Corresponding trends are small, on the order of 3-4 mm/yr, and show almost no variability, confirming that standard gridded data are inadequate to retrieve sea level variations very close to the coast.

4.3 Trends in the geophysical corrections along tracks 237 and 20 over the Jason-1/2 period; Trend comparison between track 174 and Dakar tide gauge record

To check whether the estimated near-shore trends result from real physical ocean signals rather than from spurious behavior of some altimetry corrections when approaching the coast, we computed the trends of some corrections known for being impacted by errors in the coastal zone. We focused on the wet tropospheric correction, the SSB and Dynamic Atmospheric

Correction (DAC), as these corrections are considered as less accurate in coastal areas (e.g., Cipollini et al., 2017). The same time span as above (July 2002 to June 2016) was considered. We extracted each of these corrections at the along-track SLA points located close to the coast and averaged them over successive 2-km long segments (i.e., 0-2 km, 2-4 km, etc.). We then estimated the corrections trends. Results (not shown) reveal no suspect behavior as the distance to the coast decreases. Besides, the correction trends are small and unable to explain the trend increase reported on tracks 237 and 20N (see Fig.7 and 11).

Table 2 summarizes the trend values for each correction along the two 2-km long segments for tracks 237 and 20N (a similar analysis has been performed for several other tracks, showing similar results).

Table 2: trends in geophysical corrections close to the coast (in mm/yr)

Geophysical correction trends (mm/yr) over the Jason-1/2 period	Track 237 0-2 km to coast	Track 237 2-4 km to coast	Track 20N 0-2 km to coast	Track 20N 2-4 km to coast
Wet tropospheric correction	-1.14	-0.81	-2.1	-1.86
Sea state bias (SSB)	0.21	0.46	-0.32	0.1
Dynamic atmospheric correction (DAC)	-0.26	-0.19	-0.42	0.19

As mentioned above, there is a single tide gauge record at Dakar (Senegal) with sufficiently long time series to inter-compare the altimetry-based trends computed in this study and the tide gauge-based sea level trend. Unfortunately, there is a data gap in the Dakar tide gauge record during the Jason-1 time span. Thus the comparison can only be performed over the Jason-2 period. Tide gauge data availability led us to consider the period from July 2009 to June 2016 (7 years). We used monthly RLR tide gauge data from the Permanent Service for Mean Sea Level (www.psmsl.org). The data are not corrected for vertical land motions. The trend at the tide gauge (located in the Dakar harbor) amounts to 0.90 +/- 1.35 mm/yr over this time span. The trend estimate at the closest valid point to coast (distance equal to 2.5 km) on track 174 is 2.1 +/- 5.1 mm/yr. Although the altimetry-based trend at the closest distance to coast displays large uncertainty, the two trend values agree within their respective error bars. In addition, because of lack of vertical land motion estimate at the tide gauge during this 7 years period, we cannot expect to obtain perfect agreement.

5. Discussion

In this study, for the first time, we provide decadal sea level trends very close to the coast of Western Africa, using high-resolution (20 Hz) altimetry data, based on ALES retracked waveforms inserted into the XTRACK altimetry data processing system. Over the Jason-1 and Jason-2 period (2002-2016), estimated trends along the Jason tracks show interesting behaviors from offshore towards the coast. In most instances, the trends are roughly constant from 15 km to ~ 5 km to the coast, then change significantly when approaching the coast. At some locations, a slight trend decrease is observed within the 0-4 km band followed by a sharp trend increase when approaching the coast. Such a behavior is definitely associated to coastal processes that were not visible with former altimetry products (e.g., Cazenave et al., 2017, Birol et al., 2017). This may be the result of wind-induced setup, river freshwater runoff, or wave forcing on shallow shelves (e.g., Piecuch et al., 2018, Durand et al., 2019, Melet et al., 2018). At embayed coasts and estuaries and shallow areas, cross-shore winds can drive important surge, such as observed off Senegal over the wide shelf during winter upwelling (Capet et al., 2017). Large river fresh water plumes can change water density and affect coastal sea level (e.g. Han and Webster, 2002; Brammer, 2014, Piecuch et al., 2018, Durand et al., 2019). Waves radiate energy over long distances in deep water without any perceptible signature on open ocean sea level (Hoeke et al., 2013). Their influence increases while their interaction with the bathymetry gradually increases in the near-shore where they dissipate energy. This induces a set down in the shoaling zone and setup after the breakpoint that generally reach 20 % of offshore wave height (Bowen et al., 1968). Amazingly, this is what we observed in the trends along tracks 9, 85, 161 and 237. Waves have been recently shown to strongly influence sea level trends at the coast in many regions of the world (Melet al., 2018) and in particular in the Gulf of Guinea (Melet et al., 2016) and Senegal coast (Almar et al., 2019).

Only 3 tracks show trend decrease within the 0-5 km to the coast. This is particularly clear on track 211 crossing the coast close to the Niger River estuary. Influence of the river plume could be at the origin of the observed behavior. This again will be the object of a future study.

Among the 24 Jason track portions covering the study region, 19 tracks allow estimating trends as close as 2-3 km to the coast. For 3 of them, distances of ~1 km or less are reached.

The new data provided in this study reveal unsuspected trends close to the coast, likely a result of small-scale processes occurring in the coastal zone. This represents a real progress compared to what is available with standard altimetry data, for which such an information is not available.

More investigation is needed to explain the observed trends very close to the coast. In an in-coming study, we indeed intend to explore systematically to what extent small-scale coastal processes, e.g., trend in waves and fresh water input from rivers, can explain the sharp trend increase or decrease observed at a number of locations within the last 5 km to the coast.

Planned future work will follow several directions: (1) extend the Jason sea level time series beyond 2016, using Jason-3 in particular, to estimate trends on longer periods (2) provide coastal sea level time series from Envisat and SARAL/Altika missions in order to increase the cross-track resolution and explore additional coastal areas, (3) use of SAR altimetry on Sentinel 3A and 3B to obtain sea level time series and associated trends in coastal zones with higher along-track resolution, and (4) consider a broader range of coastal zones (northern Europe, Indian continent, southeast Asia, Australia, small tropical islands). In parallel, we will interpret coastal trend behaviors in terms of coastal processes, focusing first on the western African region.

The new coastal sea level data set developed in this study will be freely available for a wide range of additional investigations, including studies of small-scale shelf currents.

Acknowledgements: This study is an outcome of the ESA CCI Sea Level 'Bridging Phase' project dedicated to coastal sea level. Florence Marti is supported by an ESA engineer grant in the context of this project.

References

Abessolo Ondoa G., R. Almar, B. Castelle et al., 2019. On the use of shore-based video camera to monitor sea level at the coast: A case study in grand popo, benin (gulf of Guinea, west Africa). Submitted to *Journal of Atmospheric and Oceanic Technology*.

Ablain M., Legeais J.F., Prandi P., et al., 2017. Altimetry-based sea level, global and regional, *Surveys in Geophysics*, 38, 7-31, DOI 10.1007/s10712-016-9389-8.

Ablain, M., Cazenave, A., Larnicol, G. et al., 2015. Improved sea level record over the satellite altimetry era (1993–2010) from the Climate Change Initiative project, *Ocean Sci.,* 11, 67-82, doi:10.5194/os-11-67-2015.

Almar, R., E. Kestenare, J. Reyns, J. et al., 2015. Response of the Bight of Benin (Gulf of Guinea, West Africa) coastline to anthropogenic and natural forcing, Part1: Wave climate variability and impacts on the longshore sediment transport, *Continental Shelf Research*, 110, 48-59.

Almar, R., Kestenare, E., Boucharel, J., 2019. On the key influence of remote climate variability from Tropical Cyclones and South Atlantic storms on the Senegalese coast (West Africa), submitted to *Environmental Research Letters*.

Angnuureng, D.B., Appeaning Addo, K., Almar, R. et al., 2017. Influence of sea level variability on a microtidal beach, *Natural Hazards*, 93(3), 1611-1628.

Anthony, E.J., Almar, R., Besset, M. et al., 2018. Response of the Bight of Benin (Gulf of Guinea, West Africa) coastline to anthropogenic and natural forcing, Part 2: Sources and patterns of sediment supply, sediment cells, and recent shoreline change. *Continental Shelf Research*, 173, 93-103.

Benveniste J., Cazenave A., Vignudelli S. et al., 2019. Requirement of a coastal zone observing system, in revision, *Frontiers in Marine Sciences*.

Birol F., N.X Fuller, F. Lyard, et al., 2017. Coastal applications from nadir altimetry: example of the X-TRACK regional products. *Advances in Space Research*, 59, 936-953, 10.1016/j.asr.2016.11.005.

Bowen, A.J., Inman, D.L., Simmons, VP., 1968. Wave 'set-down' and set-Up., *J. Geophys. Res*. 73, 2569–2577.

Brammer, H., 2014. Bangladesh's dynamic coastal regions and sea-level rise, *Climate Risk Management*, 1, 51-62.

Brown S., Kebede A.S. and Nicholls R., 2011. Sea level rise and impacts in Africa, 2000 to 2100, Technical Report, 215 pages..

Capet, X., Estrade, P., Machu, E., 2017. On the dynamics of the southern senegal upwelling center: Observed variability from synoptic to superinertial scales. *Journal of Physical Oceanography,* 47(1), 155-180.

Carrere, L. and Lyard, F. 2003. Modeling the barotropic response of the global ocean to atmospheric wind and pressure forcing- comparisons with observations. *J. Geophys. Res*. 30 (6), 1275. http://dx.doi.org/ 10.1029/2002GL016473.

Cartwright, D. E. and R. J. Taylor, 1971. New computations of the tide-generating potential, *Geophys. J. R. Astron. Soc*., 23, 45-74.

Cazenave A., Le Cozannet G., Benveniste J. et al., 2017. Monitoring the change of coastal zones from space, *EOS*, *98,* https://doi.org/10.1029/2017EO085581. Published on 02 November 2017.

Cazenave A., Palanisamy H. and Ablain M., 2018. Contemporary Sea level changes from satellite altimetry; What have we learned? What are the new challenges? *Advances in Space Research*, published online 25 July 2018, https://doi.org/10.1016/j.asr.2018.07.017.

Cipollini P., J. Benveniste, F. Birol, et al., 2018. Satellite altimetry in coastal regions. In 'Satellite altimetry over the oceans and land surfaces', Stammer & Cazenave Edts, CRC Press, Taylor and Francis Group, Boca Raton, London, New York, pp 343-373.

Dada, O.A., Agbaje, A.O., Adesina, R.B., et al., 2019. Effect of coastal land use change on coastline dynamics along the Nigerian Transgressive Mahin mud coast. *Ocean and Coastal Management*, 168, 251-264.

Durand F., Piecuch C., Cirano M. et al., 2019. Impact of continental freshwater runoff on coastal sea level, *Surveys in Geophysics*, in press.

Escudier P., Couhert A., Mercier F. et al., 2018. Satellite radar altimetry: principle, accuracy and precision, in 'Satellite altimetry over ocean and land surfaces', Stammer & Cazenave editors, CRC Press, Taylor and Francis Group, Boca Raton, London, New York, pp 1-62.

Global Climate Observing System (GCOS), 2011. Systematic observation requirements for satellite-based data products for climate (2011 update) – supplemental details to the satellite-based component of the "Implementation plan for the global observing system for climate in support of the UNFCCC (2010 update)", GCOS-154 (WMO), available at: https: //library.wmo.int/opac/doc_num.php?explnum_id=3710 (last access: 10 August 2017).

Giardino, A., Schrijvershofa, R., Nederhoffa, C.M. et al., 2016. A quantitative assessment of human interventions and climate change on the West African sediment budget. *Ocean and Coastal Management*, 156, 249-265.

Gommenginger C., P. Thibaut, L. Fenoglio-Marc, et al., 2011. Retracking altimeter waveforms near the coasts, in Coastal Altimetry, S. Vignudelli, et al. (Eds.), Springer, Berlin Heidelberg, pp. 61-101, 10.1007/978-3-642-12796-0_4.

Han, W. and Webster, P. J., 2002. Forcing mechanisms of sea level interannual variability in the Bay of Bengal. *Journal of Physical Oceanography*, 32(1), 216–239.

Hoeke, R.K., McInnes, K.L., Kruger, J.C. et al., 2013. Widespread inundation of Pacific islands triggered by distant-source wind-waves. *Global Planet. Change*, 108, 128–138.

Le Cozannet G., Garcin M., Petitjean L. et al., 2013. Exploring the relation between sea level rise and shoreline erosion using reconstructions: an example in French Polynesia, *J. Coastal Research*, 65, 2137-2142, 10.2112/SI65-361.1.

Lefèvre F., Lyard F.H., Le Provost C. et al., 2002. A global tide finite element solution assimilating tide gauge and altimetric information. *Journal of Atmospheric and Oceanic Technology*, 19 (9), 1345-1356.

Legeais J.F., Ablain M., Zawadzki L. et al., 2018. An improved and homogeneous altimeter sea level record from the ESA Climate Change Initiative, *Earth Syst. Sci. Data*, 10, 281-301, https://doi.org/10.5194/essd-10-281-2018.

Luijendijk A., Hagenaars G, Ranasinghe R. et al., 2018. the state of the world beaches, *Scientific Reports*, 8, 6641, DOI:10.1038/s41598-018-24630-6.

Melet, A., Almar, R. and Meyssignac, B., 2016. What dominates sea level at the coast: a case study for the Gulf of Guinea. *Ocean Dyn.* 66, 623–636.

Melet A., Meyssignac B. Almar R. et al., 2018. Under-estimated wave contribution to coastal sea-level rise, *Nature Climate Change*, 8, 234–239.

Neumann B, Vafeidis AT, Zimmermann J. et al., 2015. Future Coastal Population Growth and Exposure to Sea-Level Rise and Coastal Flooding - A Global Assessment. *PLoS ONE* 10(3): e0118571.

Ondoa, G., Vacchi, M., 2018. Response of the Bight of Benin (Gulf of Guinea, West Africa) coastline to anthropogenic and natural forcing, Part 2: Sources and patterns of sediment supply, sediment cells, and recent shoreline change. *Continental Shelf Research*, 173, 93-103.

Passaro M., Cipollini P., Vignudelli S. et al., 2014. ALES: A multi-mission subwaveform retracker for coastal and open ocean altimetry. *Remote Sensing of Environment* 145, 173-189, 10.1016/j.rse.2014.02.008.

Passaro M., Cipollini P., Benveniste J., 2015. Annual sea level variability of the coastal ocean: The Baltic Sea-North Sea transition zone. *Journal of Geophysical Research* 120(4): 3061-3078, 10.1002/2014JC010510.

Passaro M., Zulfikar Adlan N. and Quartly G.D., 2018. Improving the precision of sea level data from satellite altimetry with high-frequency and regional sea state bias corrections. *Remote Sensing of Environment*, 245-254, 10.1016/j.rse.2018.09.007.

Piecuch C.G., Bittermann K., Kemp A.C. et al., (2018). River-discharge effects on United States Atlantic and Gulf coast sea-level changes, *PNAS*, vol. 115, no. 30, 7729–7734.

Quartly G.D., Legeais J.F., Ablain M. et al., 2017. A new phase in the production of quality-controlled sea level data, *Earth Syst. Sci. Data*, 9, 557–572, doi.org/10.5194/essd-9-557-2017.

Vessel, P., and W. H. F. Smith, 1996. A Global Self-consistent, Hierarchical, High-resolution Shoreline Database, *J. Geophys. Res., 101*, 8741-8743.

Wang, X. and Ichikawa, K., 2017. Coastal Waveform Retracking for Jason-2 Altimeter Data Based on Along-Track Echograms around the Tsushima Islands in Japan. *Remote Sens*. 9, 762.

Wahr, J.M., 1985. Deformation Induced by Polar Motion. *J. Geophys. Res.,* 90 (B11), 9363–9368.

Wong, P., Losada I.J., Gattuso J.P. et al., 2014. Coastal systems and low-lying areas. In: Climate Change 2014: Impacts, Adaptation, and Vulnerability. Part A: Global and Sectoral Aspects. Contribution of Working Group II to the Fifth Assessment Report of the Intergovernmental Panel on Climate Change [Field, C.B. et al. (eds.)]. *Cambridge University Press*, Cambridge, United Kingdom and New York, NY, USA, pp. 361-409.

Woodworth P., Melet A., Marcos M. et al., 2019. Forcing Factors Causing Sea Level Changes at the Coast, *Surveys in Geophysics*, in press.

Xu X.Y., Birol F. and Cazenave A., 2018. Evaluation of Coastal Sea Level of Jason-2 Altimetry Offshore Hong Kong, *Remote Sensing*, 10, 282, doi:10.3390/rs10020282.

Figure captions

Fig.1 Regional sea level trends over the altimetry era (1993-present) from the Copernicus Climate Change Service (C3S) sea level products

Fig.2: Gloss-based tide gauge network coverage along world coastlines with >40 years records

Fig.3: Radar altimetry waveforms from the Jason-2 satellite in different ocean environments (blue curves) and superimposed ALES retracking model (dashed red curves) (adapted from Passaro et al., 2014)

Fig.4: Sea level trends from the C3S gridded product over July 2002 to June 2016 over the study region. Jason tracks (identified by numbers) are superimposed

Fig.5: Sketch illustrating the method to compute the distance to the coast. The dashed line represents the mean track profile. The thick solid line starting from the closest point to coastline illustrates the shortest distance to coast.

Fig.6: *Track 187*. Upper left panel: Sea level trends (mm/yr; colored circles) computed over the 14-year time span at each 20 Hz point for the closest track portion to the coast (a few km). Red/white triangles identify points with non-significant trend estimates (sea level data too scattered or not enough numerous for a robust trend estimation). The background map shows the geographical setting based on a 2018 version of Google Earth. Upper right panel: Associated sea level trend uncertainties (+/- 1 standard error) at each 20 Hz point along the same track as on the left hand side map (note the change in color scale). Lower plots: sea level time series (blue dots) since June 2002 for the first three 20 Hz points closest to the coast (distance indicated in the heading). Red dots are outliers identified by simple statistical test. In green is shown the regression line computed over the 14-year time span (excluding the outliers). The corresponding trend value and associated error (+/-1 standard deviation) are indicated in the legend of the figure.

Fig.7 : same as Fig.6 for *Track 237*.

Fig.8 : same as Fig.6 for *Track 33*.

Fig.9 : same as Fig.6 for *Track 174*.

Fig.10 : same as Fig.6 for *Track 46*.

Fig.11 : same as Fig.6 for *Track 20*.

Fig.12: Sea level trend values (in mm/yr) and associated formal errors (+/- 1 standard deviation; shaded area) as a function of distance to the coast (last 15 km) estimated at each 20 Hz point, for all 24 Jason track portions considered in this study. Plots are ranked for all ascending tracks first, then all descending tracks.

Fig.13: Sea level trend errors (in mm/yr) computed at each 20 Hz point along the last 50 km distance to coast for track 187 (a) and track 20N (b).

Fig.14: Distribution of the closest distance to coast (in km) of the first valid 20 Hz point for all 24 Jason track portions considered in the study region (black/grey bars correspond to ascending/descending tracks).

Fig.15: Distribution of sea level trend values (in mm/yr) at shortest distance to coast for the 24 Jason track portions considered in this study using the XTRACK/ALES data (a). Same as (a) but using data

from the C3S grids interpolated along the Jason tracks (b). In both cases, trends are computed over July 2002 to June 2016.

Fig. 16: Left panel: sea level trends (in mm/yr) averaged over 50 km-long segments along track 148, as a function of distance to the coast (black points); The C3S trend interpolated along the track is also shown (open squares). Right panel: same as left panel but for 2 km-long segments for the last 50 km to the coast.

Figure 1

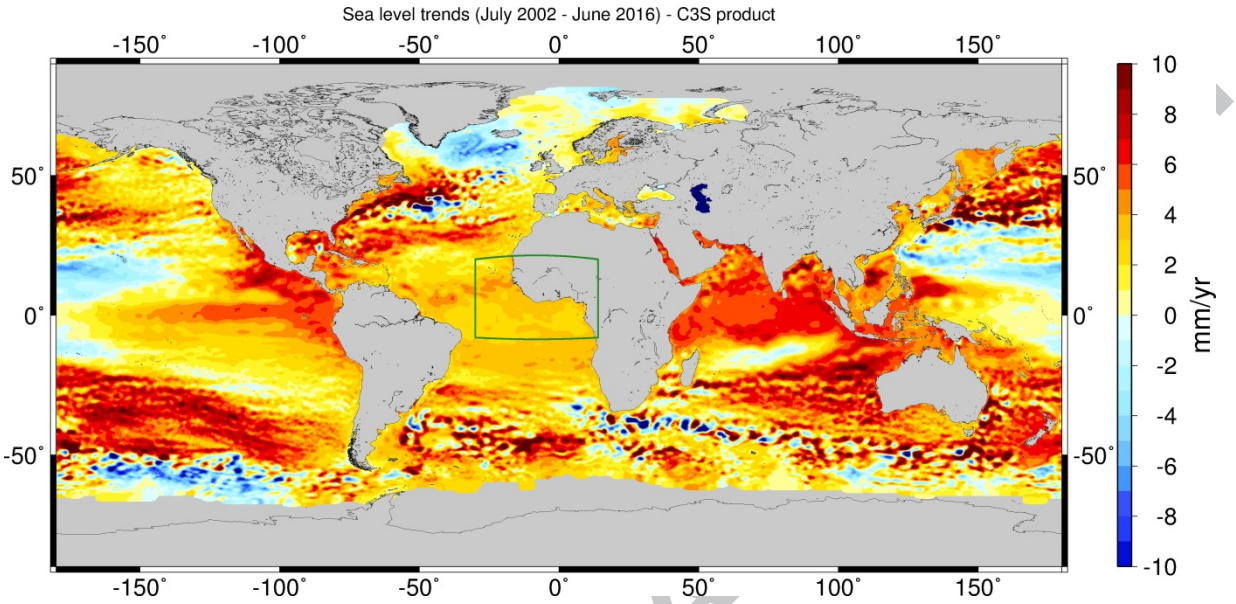

Figure 2

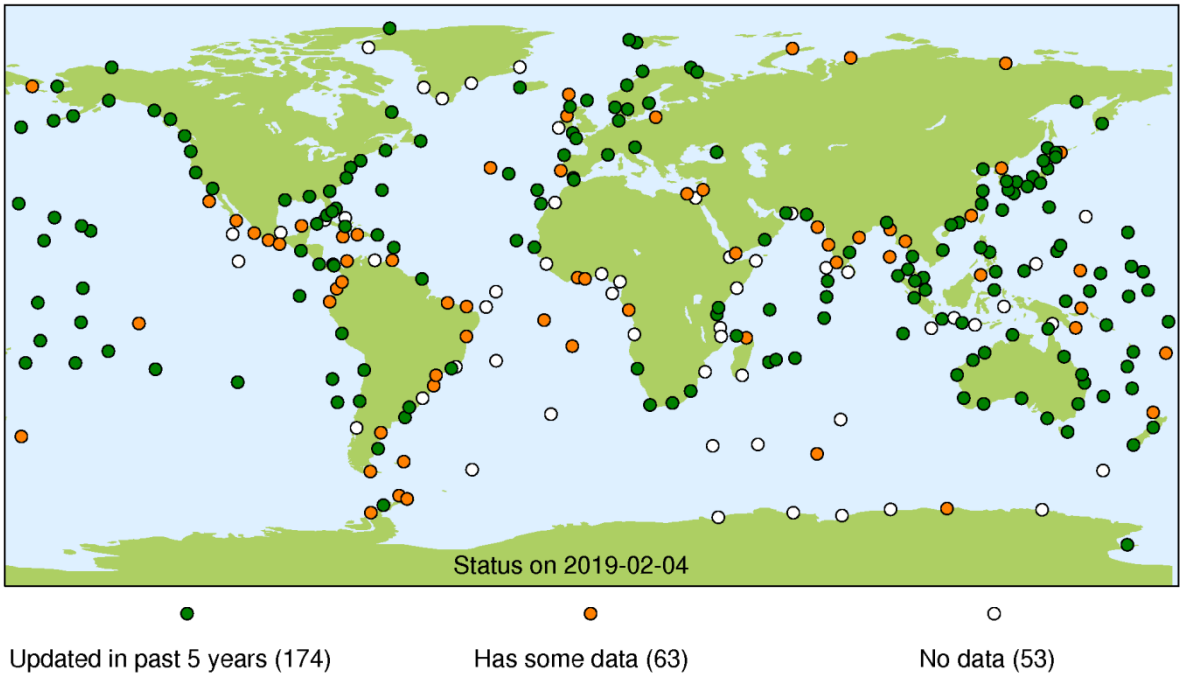

Figure 3

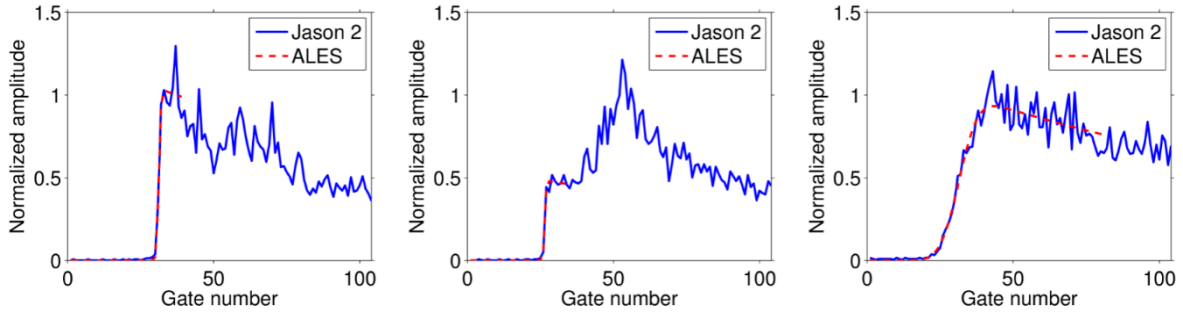

Figure 4

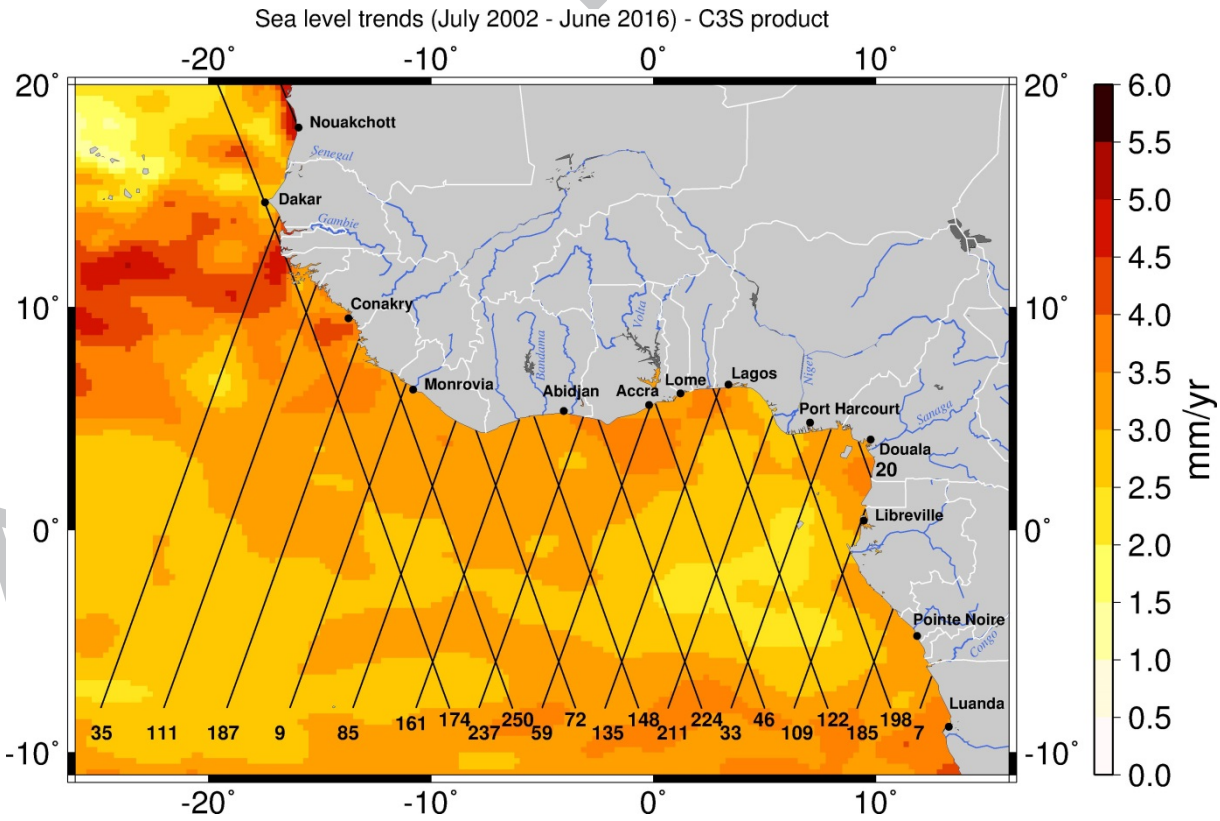

Figure 5

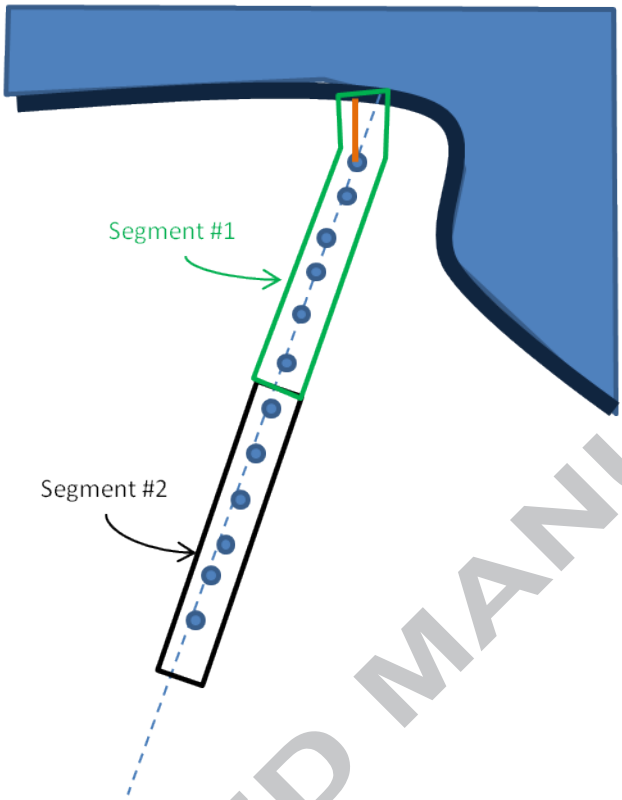

Figure 6

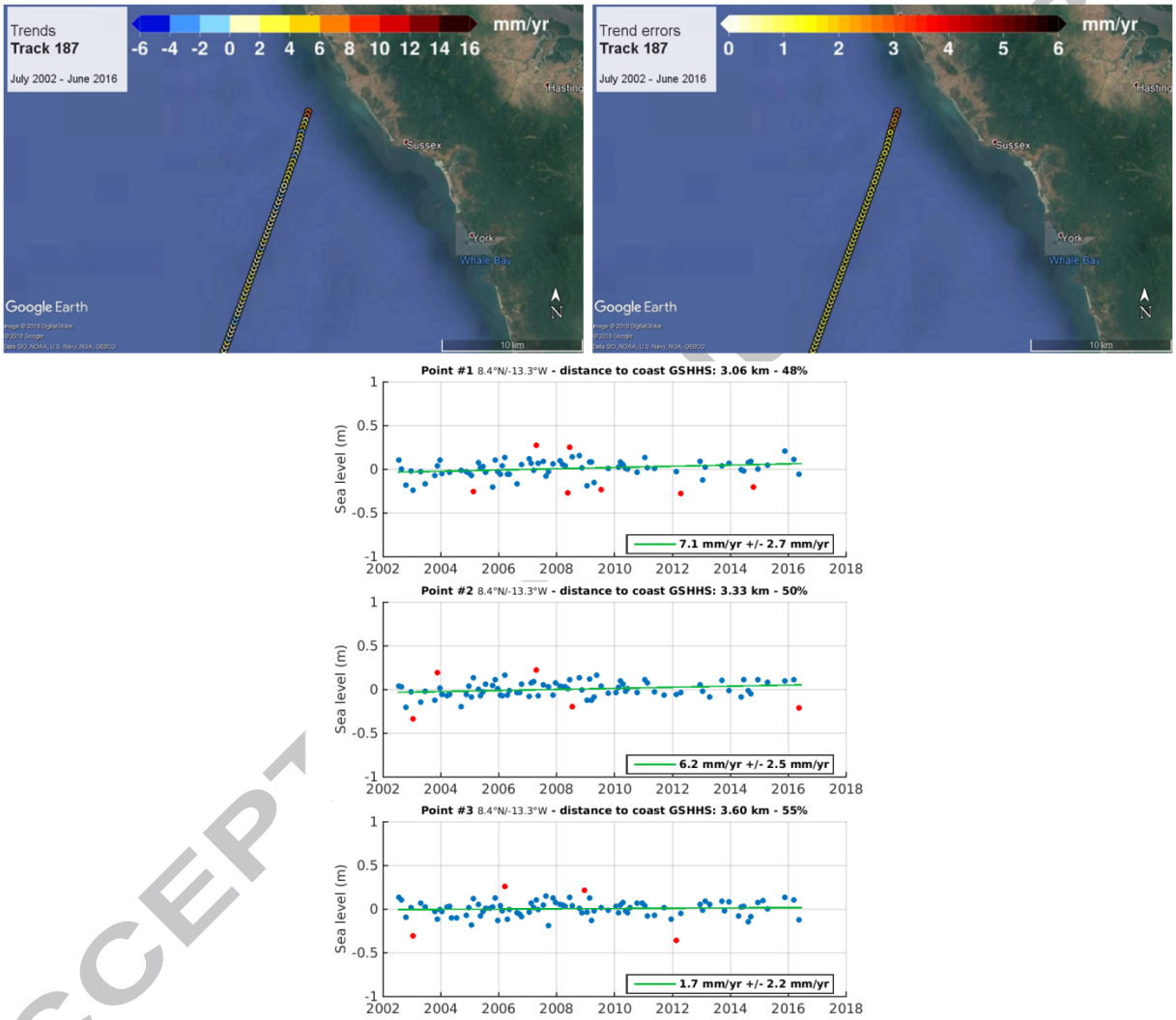

Figure 7

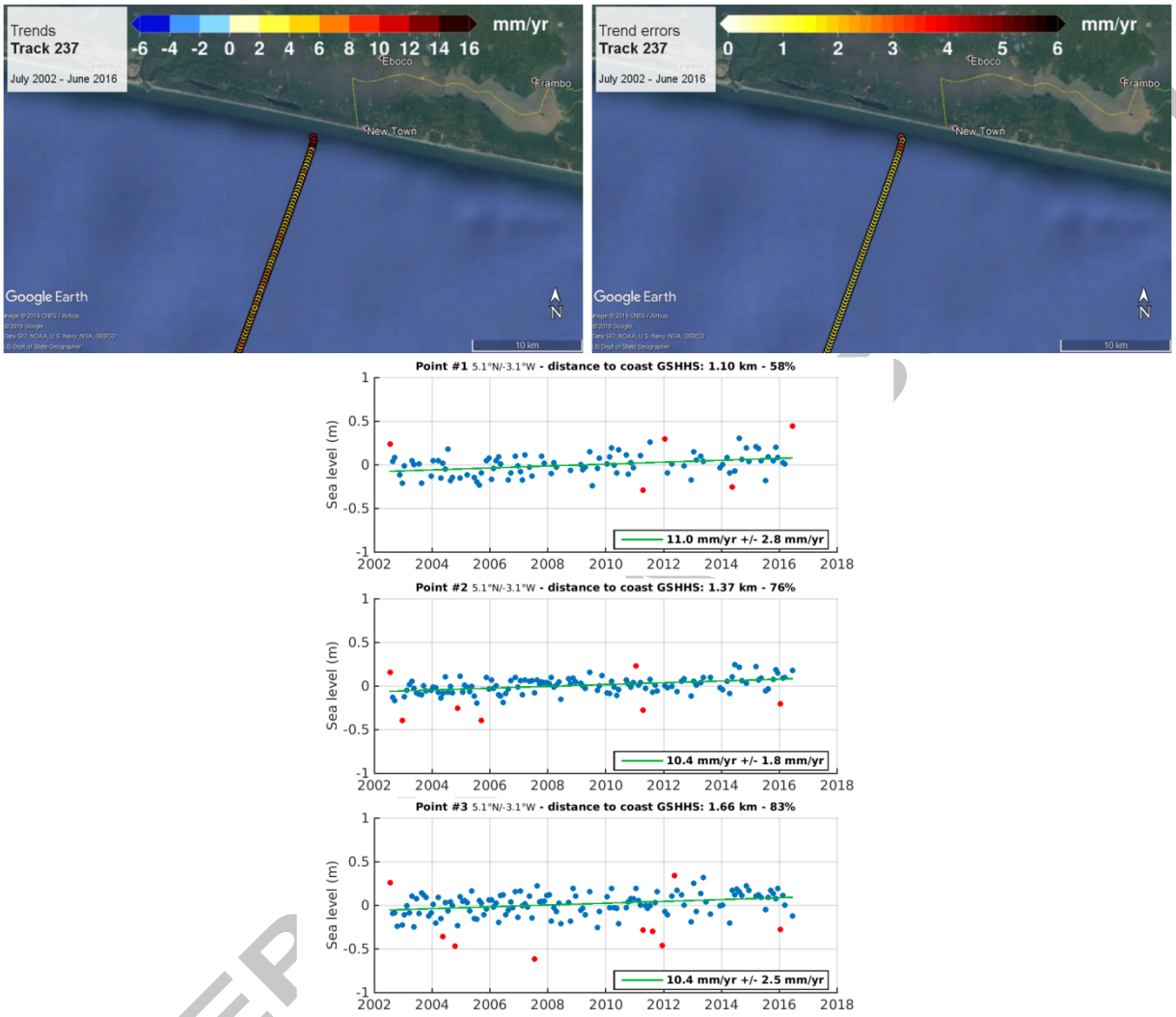

Figure 8

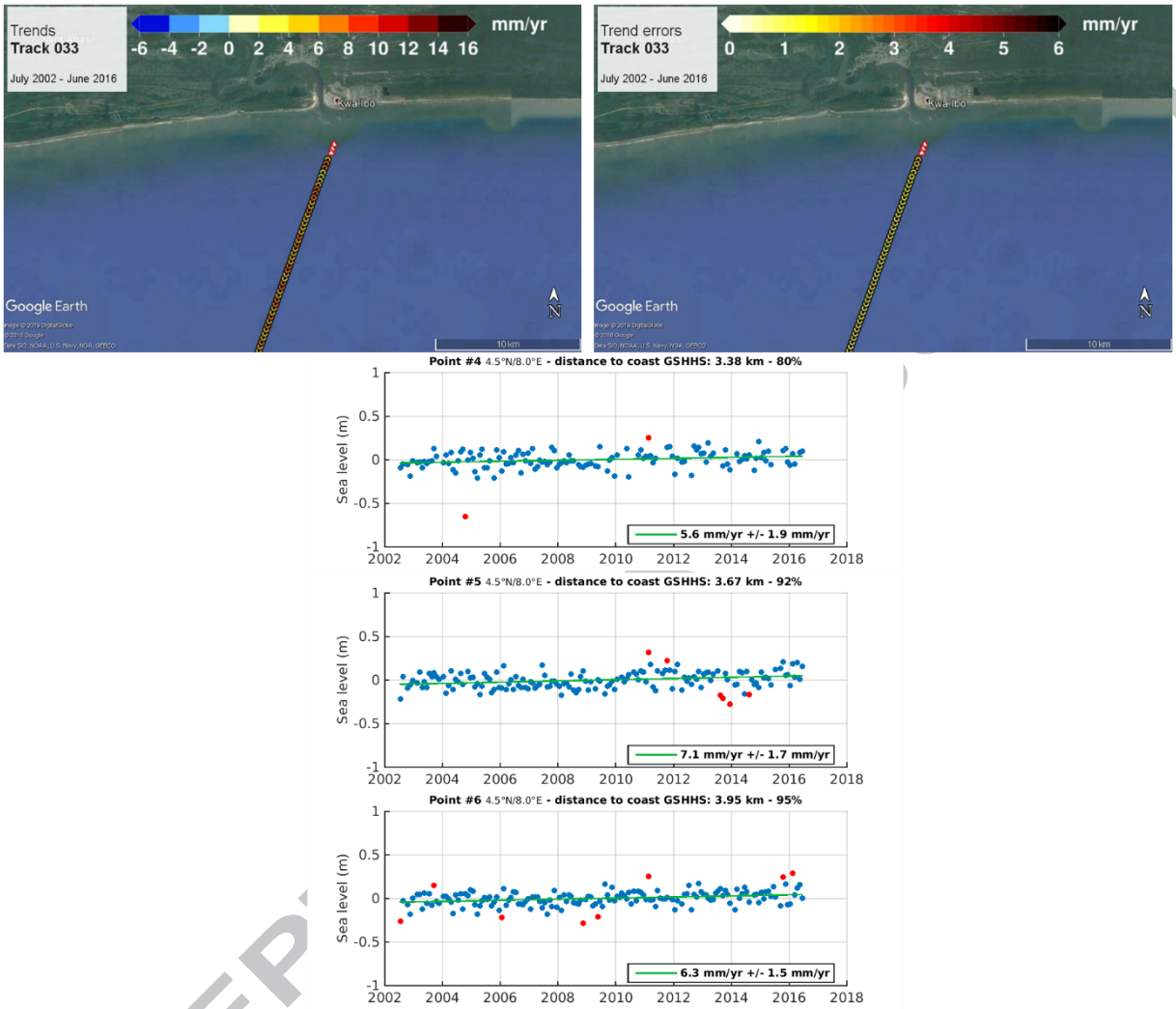

Figure 9

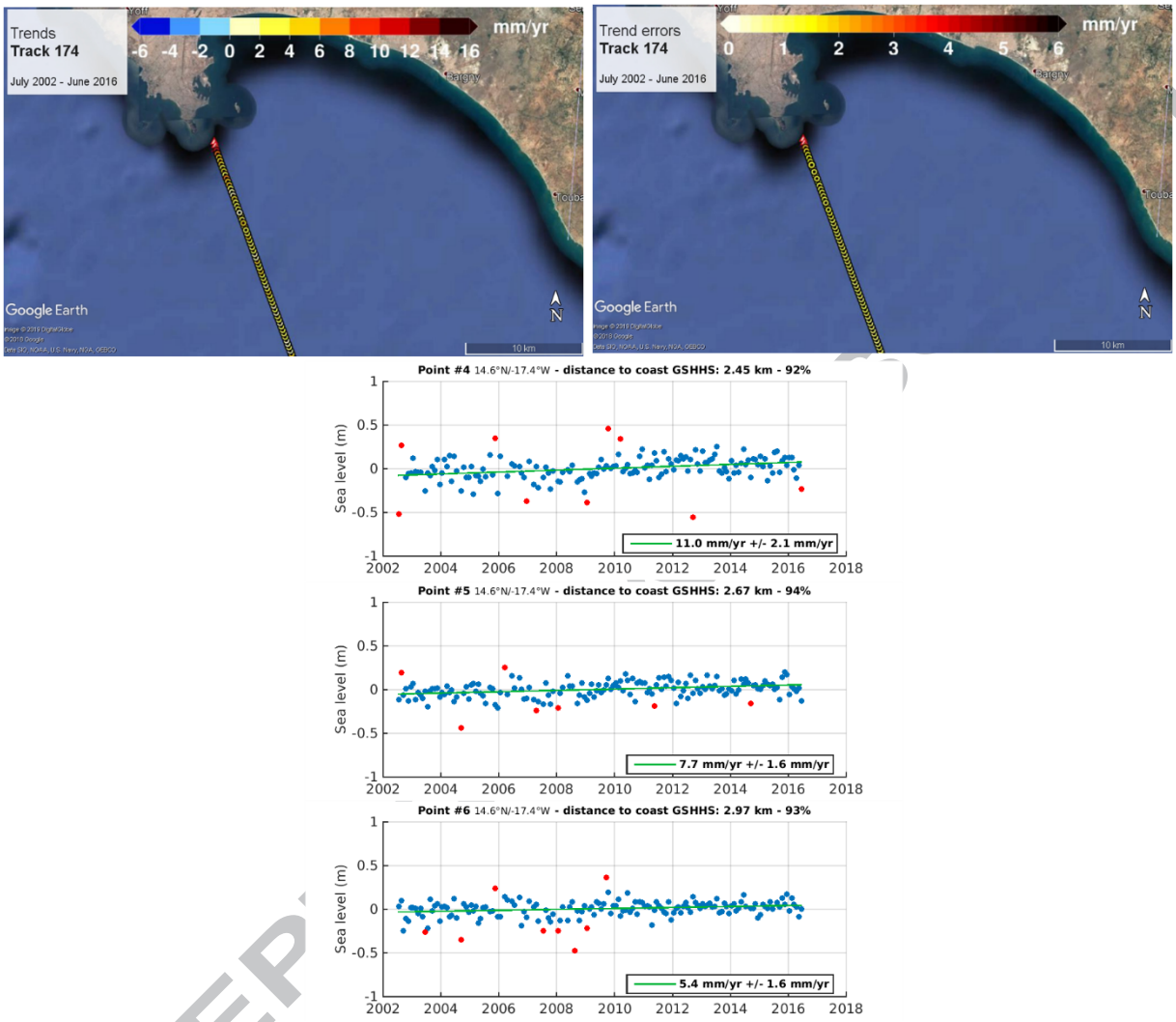

Figure 10

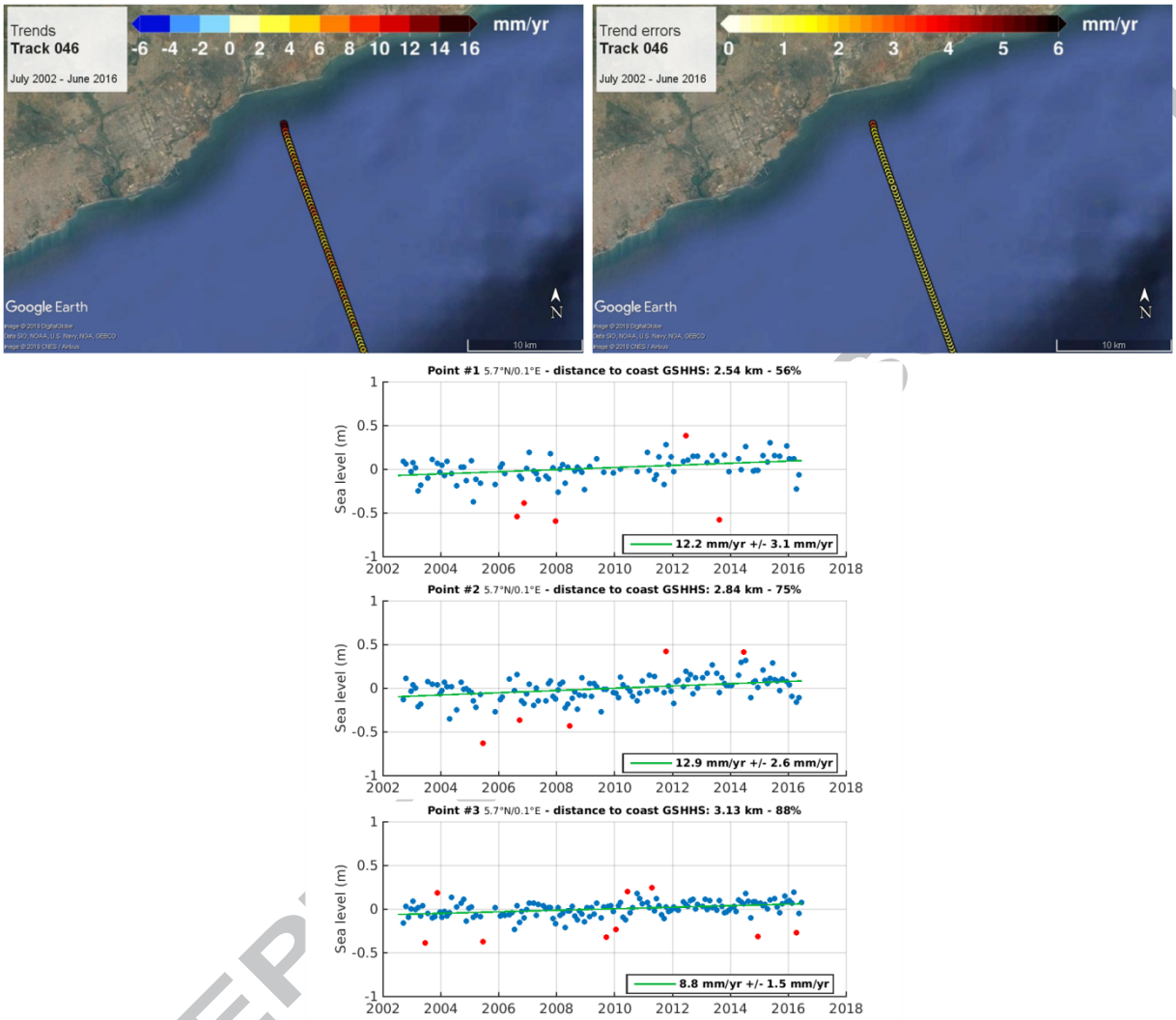

Figure 11

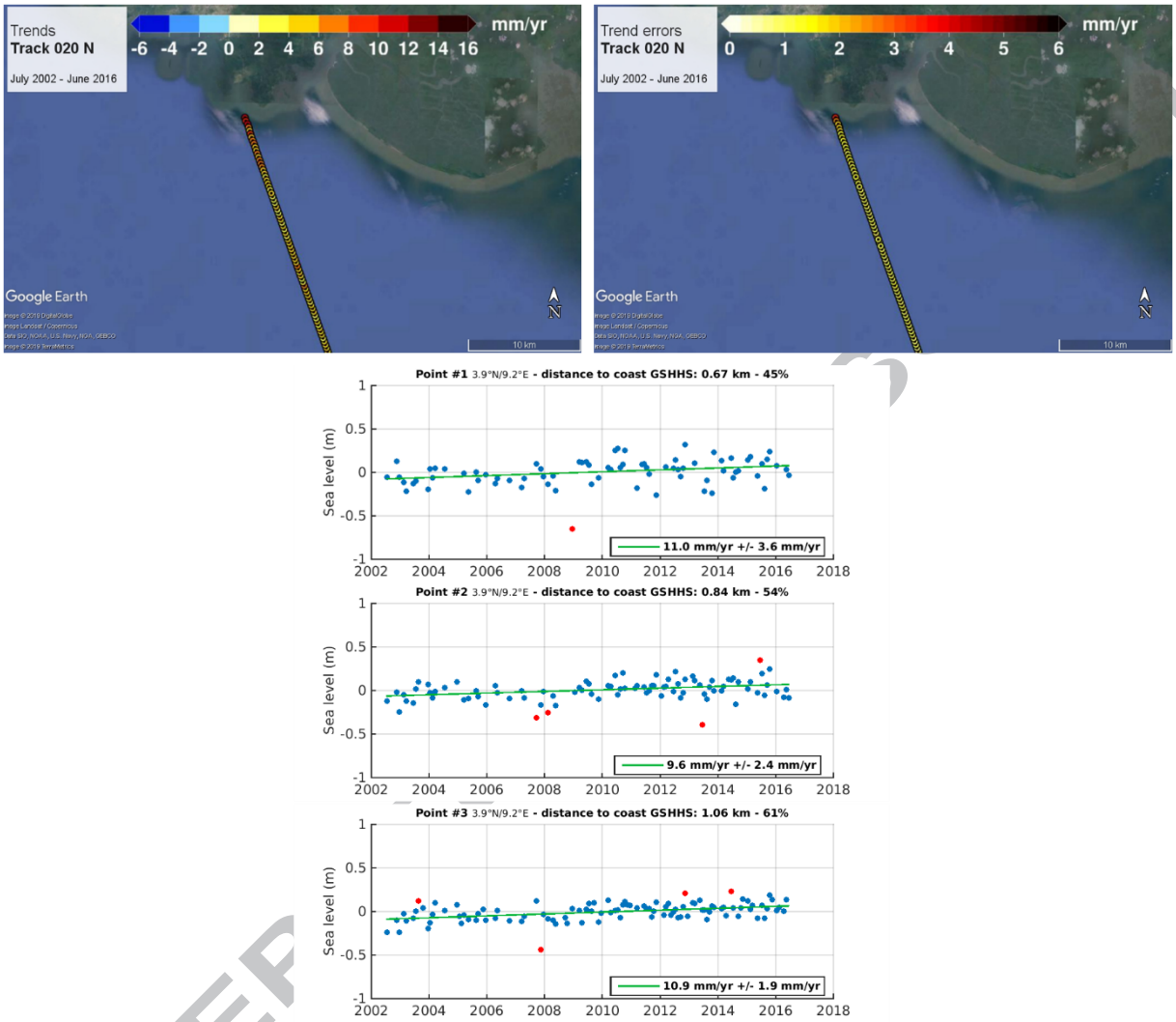

Figure 12 (1)

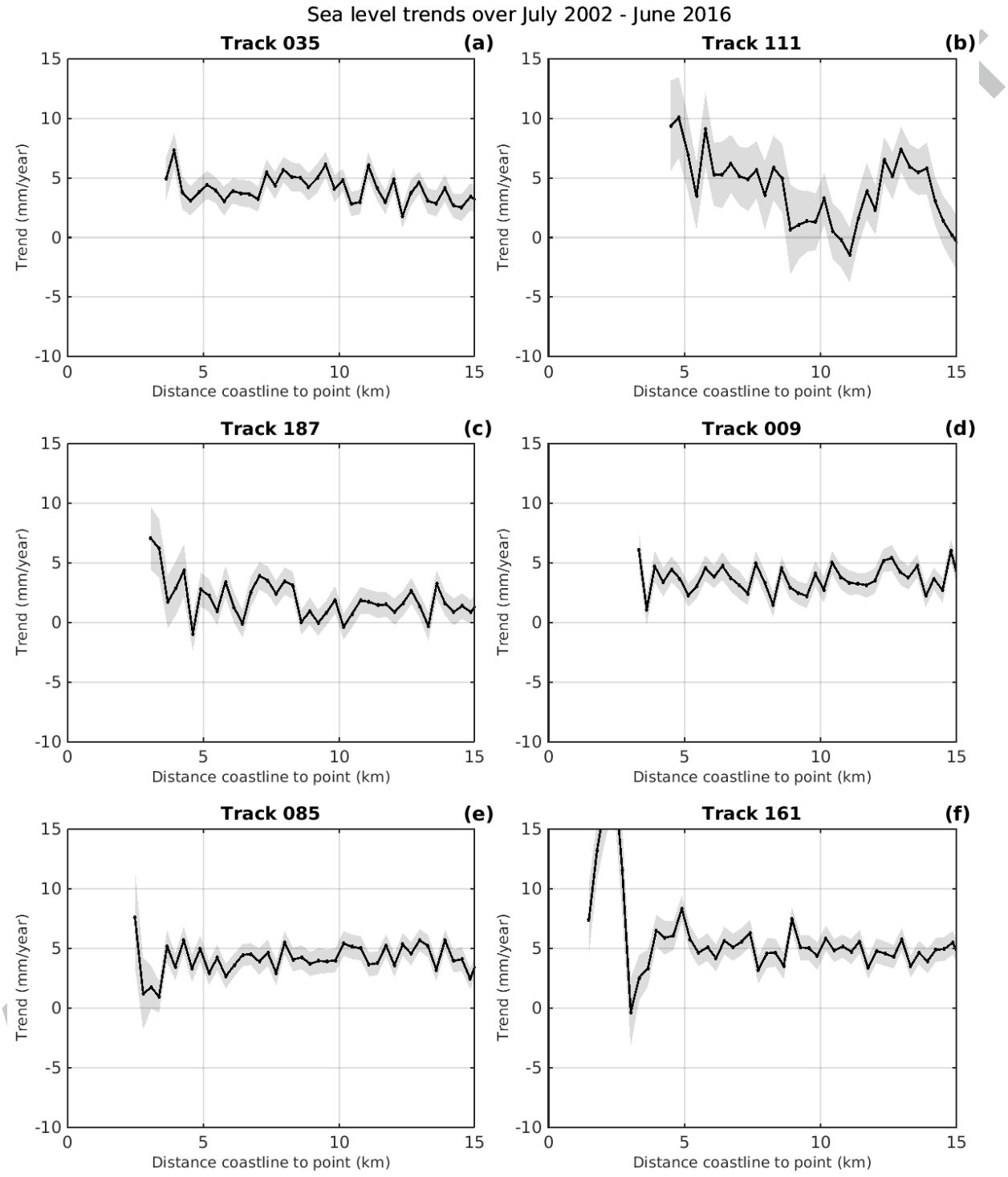
Sea level trends over July 2002 - June 2016
Track 035
(a)
Track 111
(b)
Track 187
(c)
Track 009
(d)
Track 085
(e)
Track 161
(f)
Trend (mm/year)
Distance coastline to point (km)

Figure 12 (2)

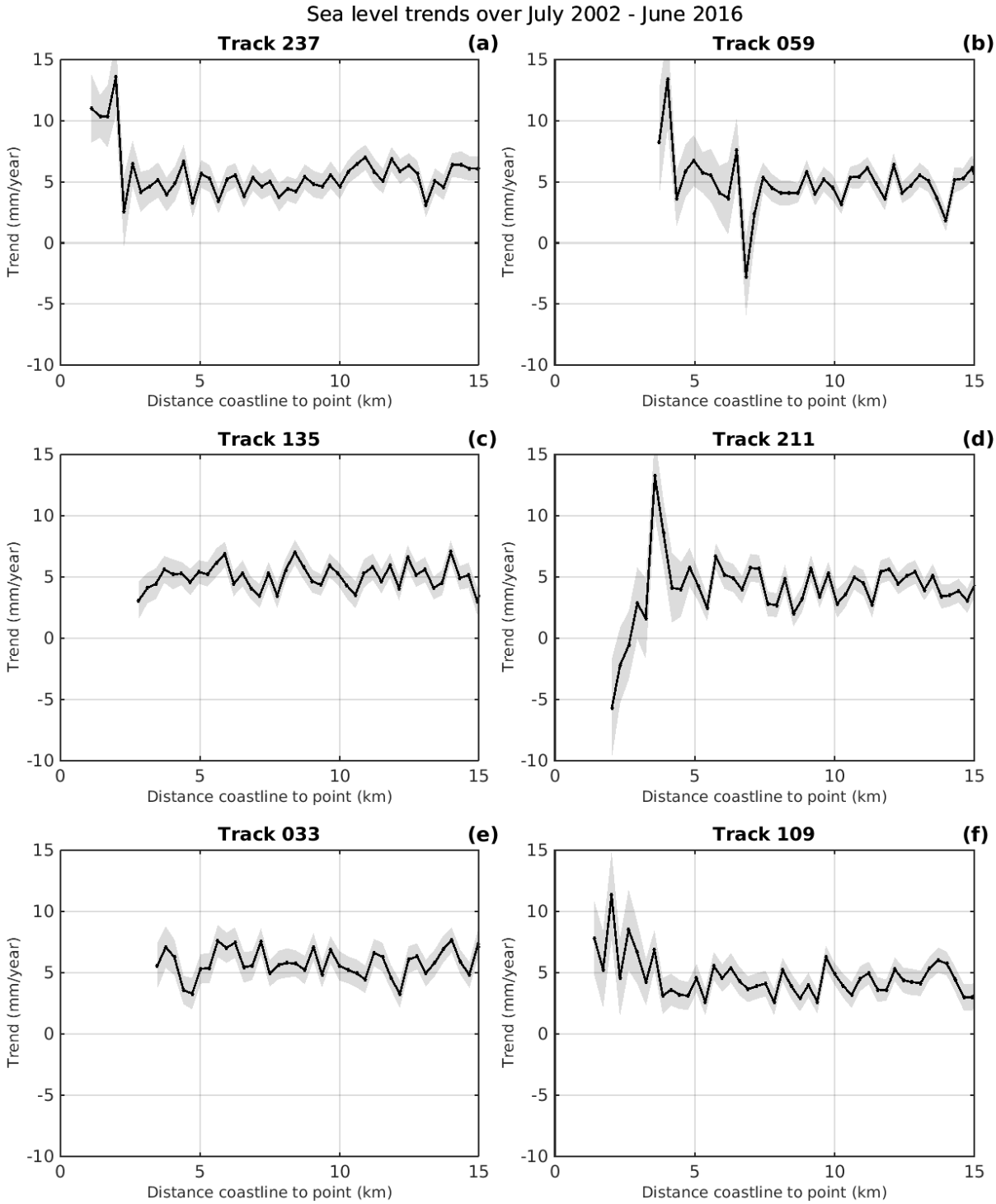

Figure 12 (3)

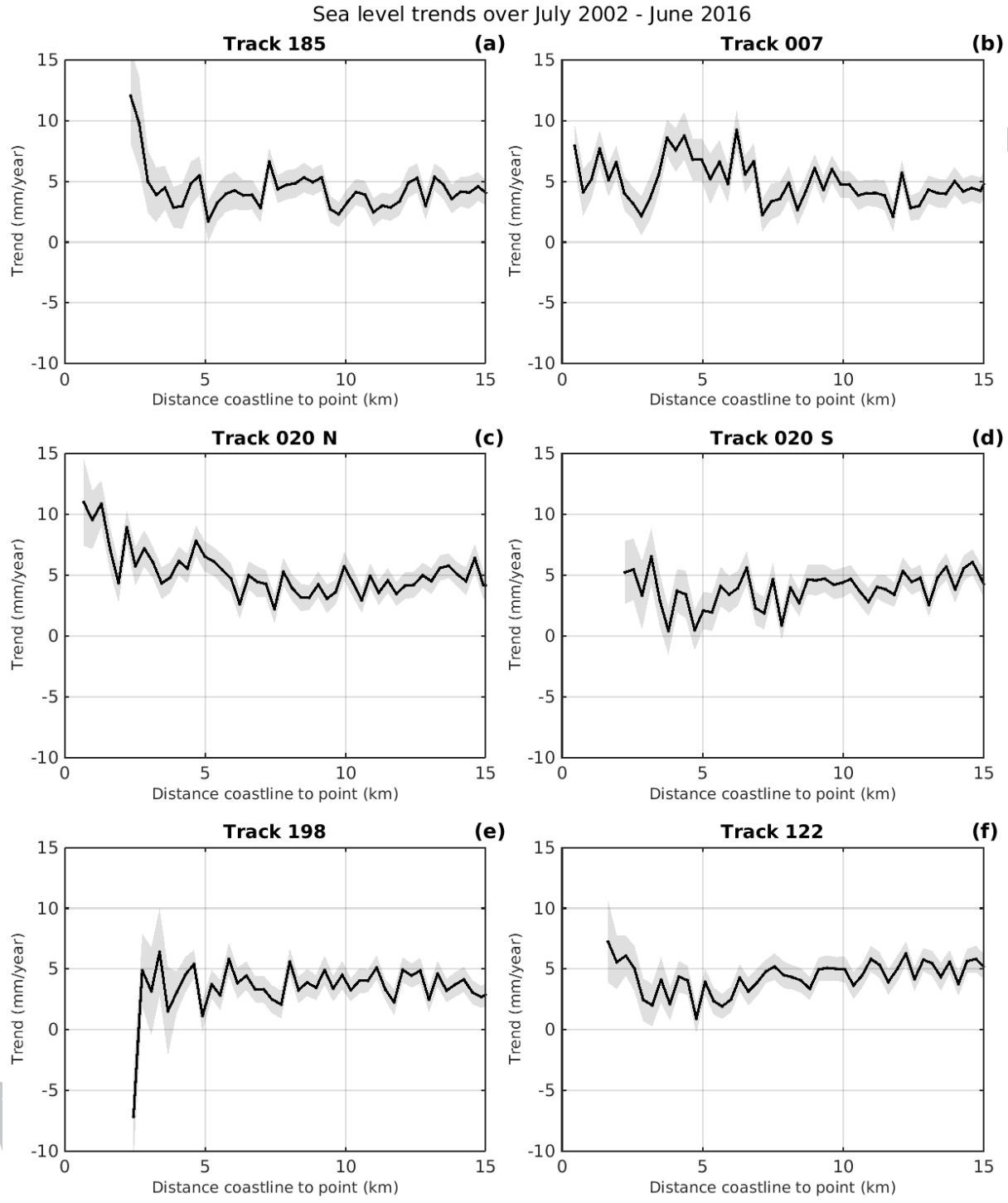

Figure 12 (4)

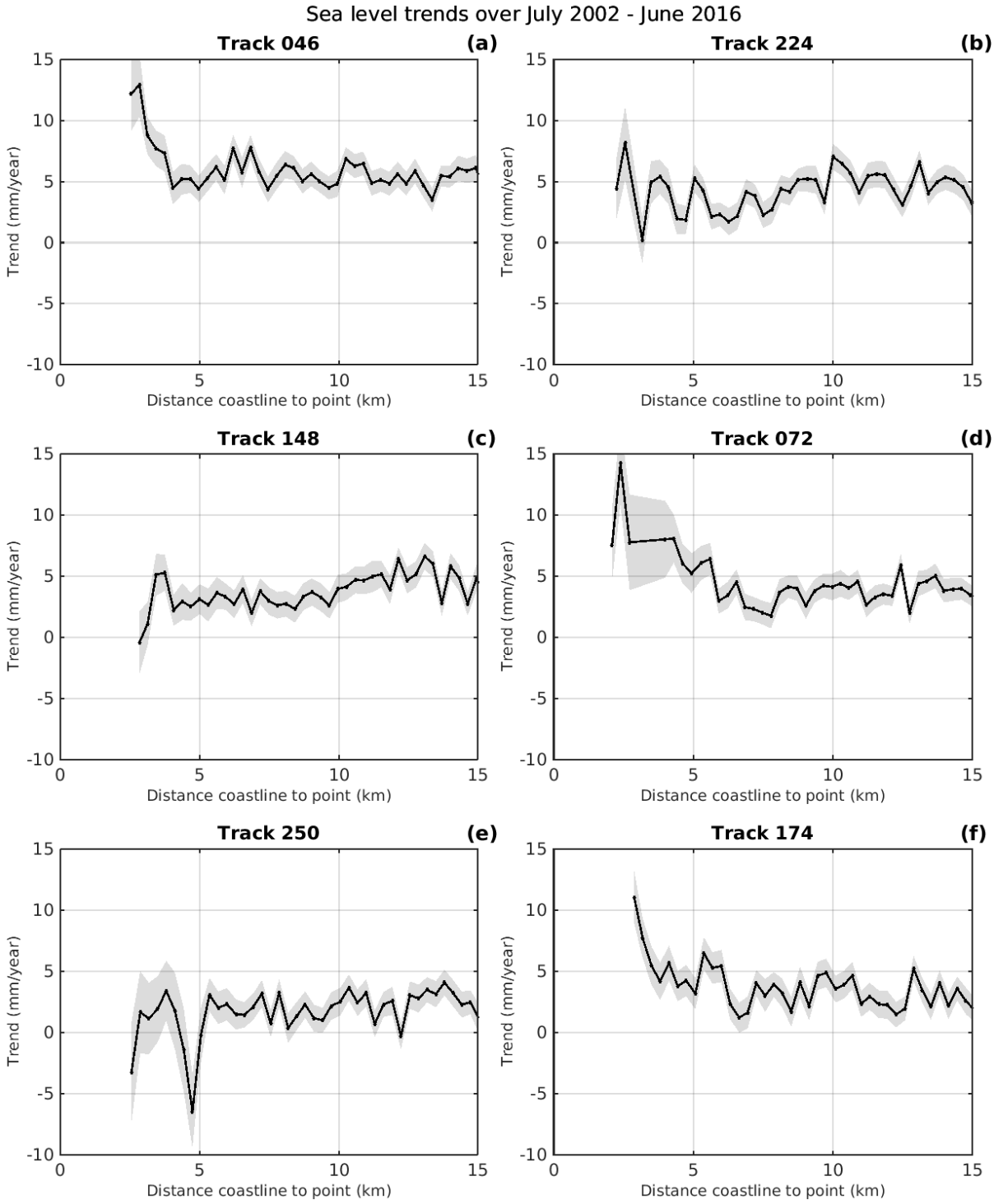

Figure 13

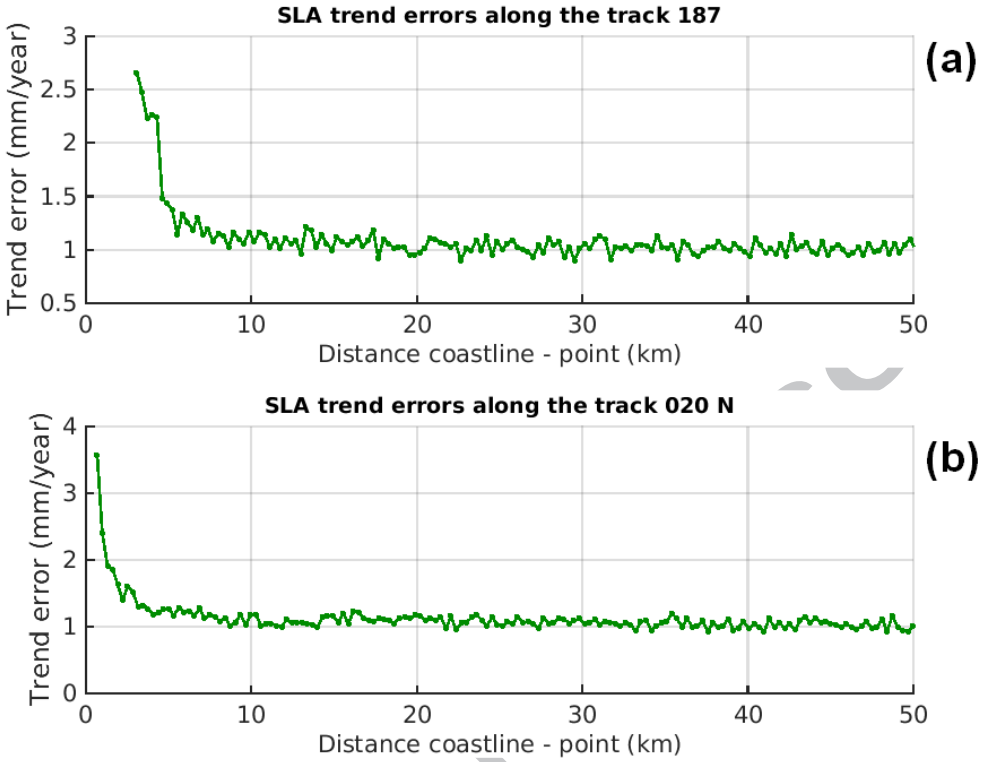

Figure 14

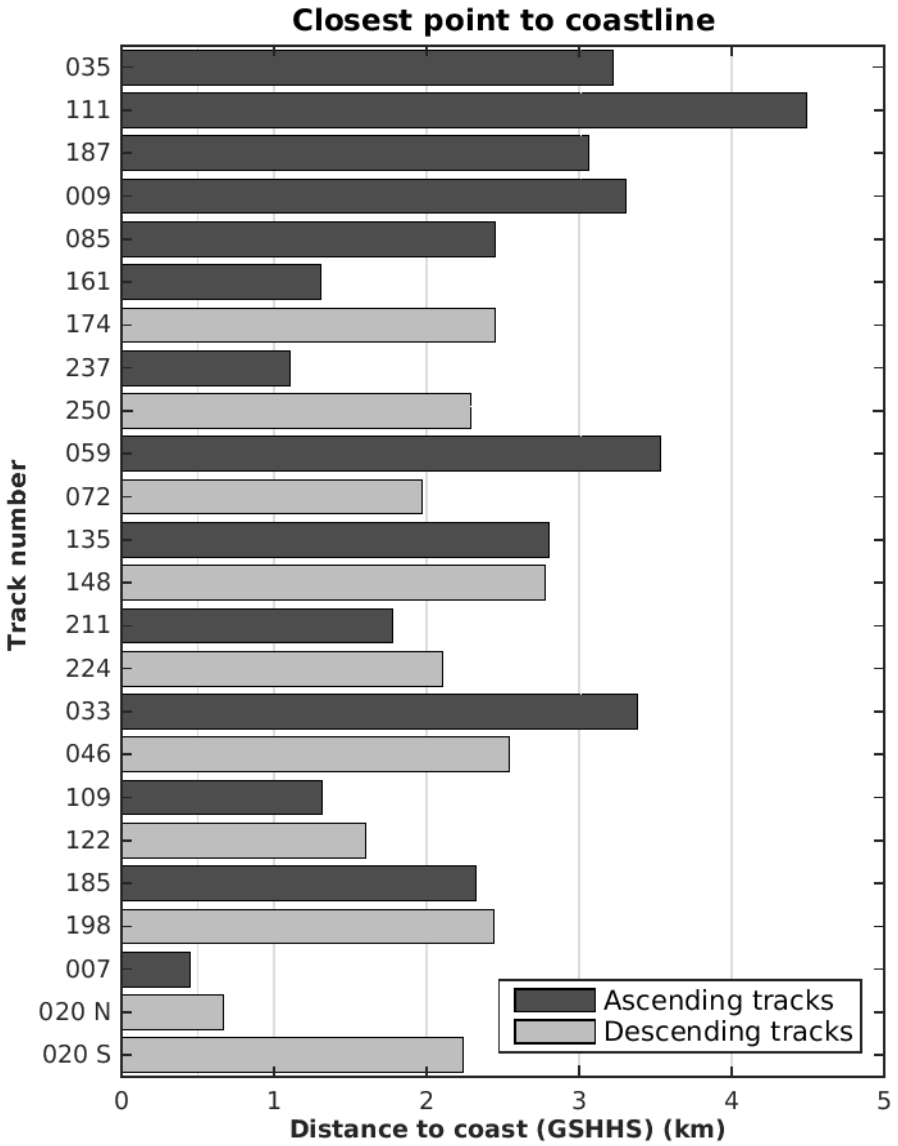

Figure 15

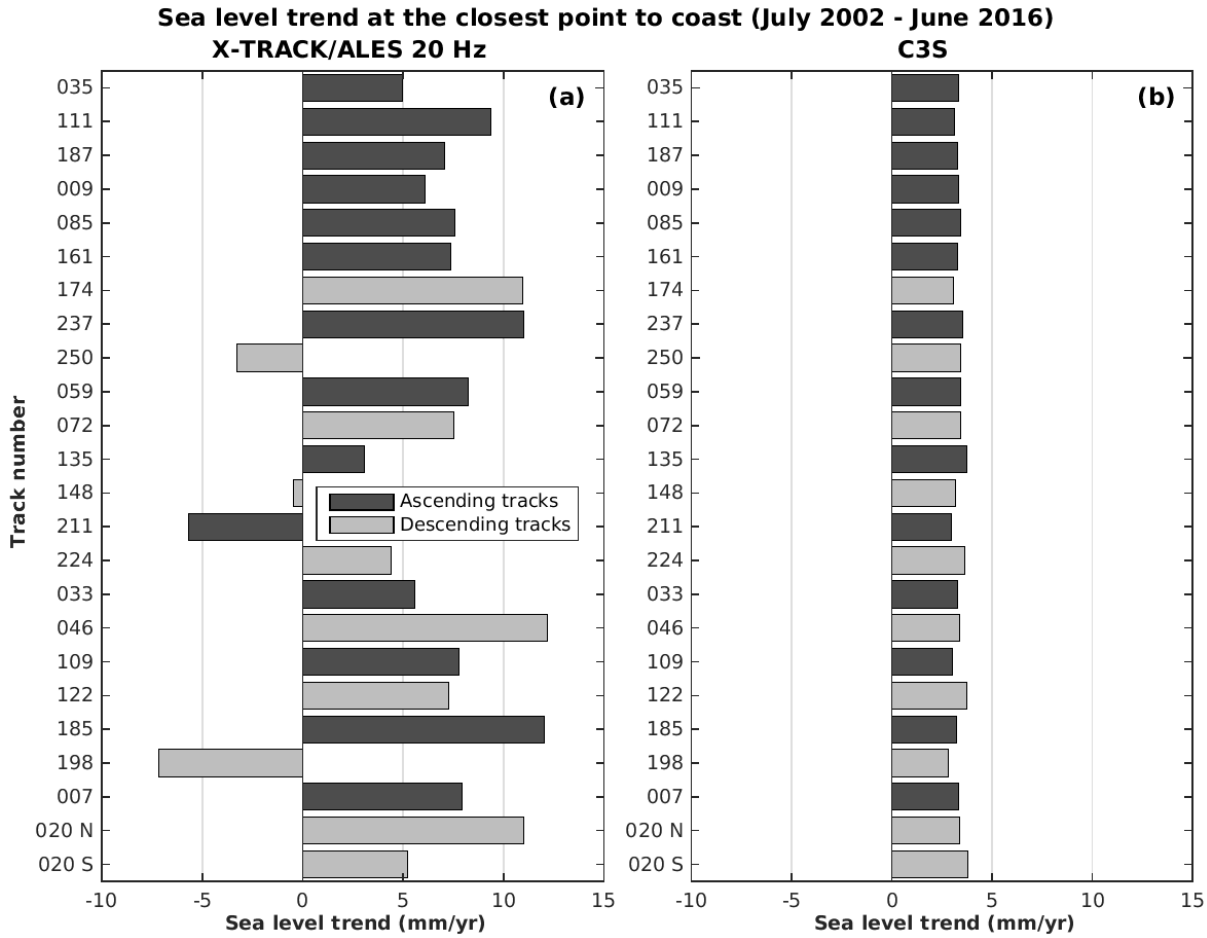

Figure 16